UDC 539.261, 620.187, 691.75
https://doi.org/10.17073/0021-3438-2023-6-35-43

Research article
Научная статья

Effect of severe plastic deformation on the structure and properties of the Zn–1%Li–2%Mg alloy

V.D. Sitdikov[1,2], **E.D. Khafizova**[2,3], **M.V. Polenok**[2,3]

[1] **LLC RN-BashNIPIneft**
86/1 Lenina Str., Ufa 450006, Russia

[2] **Institute of Physics of Molecules and Crystals of Ufa Research Center of the Russian Academy of Sciences**
151 Oktyabrya Prosp., Ufa 450075, Russia

[3] **Ufa University of Science and Technologies**
32 Zaki Validi Str., Ufa 450076, Russia

✉ Vil' D. Sitdikov (svil@ugatu.su, SitdikovVD@bnipi.rosneft.ru)

Abstract: Through the optimization of processing parameters, including pressure, temperature, and deformation degree, a high pressure torsion (HPT) regime was identified. This regime allows for the creation of a unique microstructure in the biodegradable Zn–1%Li–2%Mg alloy, which exhibits exceptional physical and mechanical properties. Following 10 revolutions of HPT treatment (resulting in an accumulated deformation degree, $\gamma = 571$) at the temperature of 150 °C and an applied pressure of 6 GPa, the Zn–1%Li–2%Mg alloy displayed notable mechanical characteristics, including a high yield strength (~385 MPa), ultimate tensile strength (~490 MPa), and ductility (44 %) during tensile tests. To elucidate the underlying reasons for these remarkable mechanical properties, an examination of the alloy's microstructure was conducted employing electron microscopy and X-ray phase analysis (XPA). The study revealed the formation of a distinct microstructure characterized by alternating bands of the α-phase Zn, a mixture of Zn and ~$LiZn_3$ phases, as well as the α-phase Zn containing Mg_2Zn_{11} particles, as a consequence of HPT treatment. Additionally, it was observed that HPT treatment induced a dynamic strain aging process, leading to the precipitation of Zn particles in the $LiZn_3$ phase and the precipitation of Mg_2Zn_{11} and β-$LiZn_4$ particles in the Zn phase. These precipitated particles exhibited a nearly spherical shape. The application of the XPA method helped to confirm that the Zn phase becomes the predominant phase during HPT treatment, and microscopy data showed the formation of an ultra-fine grained (UFG) structure within this phase. A comprehensive analysis of the hardening mechanisms, based on the newly acquired microstructural insights, revealed that enhanced strength and ductility of the Zn–1%Li–2%Mg UFG alloy can be attributed primarily to the effects of dispersion, grain boundary, and hetero-deformation-induced hardening, including dislocation strengthening.

Keywords: zinc alloy, severe plastic deformation, strength, ductility, microstructure, phase composition, *X*-ray diffraction analysis, hardening mechanisms.

Acknowledgments: The research was conducted with the support of the Russian Science Foundation Grant No. 23-29-00667, https://rscf.ru/project/23-29-00667

For citation: Sitdikov V.D., Khafizova E.D., Polenok M.V. Effect of severe plastic deformation on the structure and properties of the Zn–1%Li–2%Mg alloy. *Izvestiya. Non-Ferrous Metallurgy.* 2023;29(6):35–43.
https://doi.org/10.17073/0021-3438-2023-6-35-43

Влияние интенсивной пластической деформации на структуру и свойства сплава Zn–1%Li–2%Mg

В.Д. Ситдиков[1,2], **Э.Д. Хафизова**[2,3], **М.В.Поленок**[2,3]

[1] **ООО «РН-БашНИПИнефть»**
450006, Россия, Республика Башкортостан, г. Уфа, ул. Ленина, 86/1

[2] **Институт физики молекул и кристаллов**
Уфимского научного центра Российской академии наук
450075, Россия, Республика Башкортостан, г. Уфа, пр-т Октября, 151

[3] **Уфимский университет науки и технологий**
450076, Россия, Республика Башкортостан, г. Уфа, ул. Заки Валиди, 32

✉ Виль Даянович Ситдиков (svil@ugatu.su, SitdikovVD@bnipi.rosneft.ru)

Аннотация: Путем оптимизации параметров процессинга (давление, температура, степень деформации) найден режим интенсивной пластической деформации кручения (ИПДК), позволяющий сформировать в биоразлагаемом сплаве Zn–1%Li–2%Mg необычную микроструктуру, проявляющую уникальные физико-механические свойства. Так, после 10 оборотов ИПДК (степень накопленной деформации $\gamma = 571$), реализованной при температуре 150 °С и приложенном давлении 6 ГПа, сплав Zn–1%Li–2%Mg при испытаниях на растяжение продемонстрировал высокие показатели предела текучести (~385 МПа), предела прочности (~ 490 МПа) и пластичности (44 %). Для объяснения причин уникальных механических характеристик данного материала проанализирована его микроструктура методами электронной микроскопии и рентгенофазового анализа (РФА). Показано, что в сплаве в результате ИПДК формируется особая микроструктура, состоящая из чередующихся полос α-фазы Zn, смеси фаз Zn и ~$LiZn_3$, а также α-фазы Zn, содержащей частицы Mg_2Zn_{11}. Установлено, что при обработке ИПДК также реализуется процесс динамического старения, в результате которого в фазе ~$LiZn_3$ выпадают частицы Zn, а в фазе Zn – Mg_2Zn_{11} и β-$LiZn_4$. При этом показано, что эти частицы по форме близки к сфере. Методом РФА также установлено, что при обработке ИПДК основной становится фаза Zn, в которой, по данным микроскопии, формируется ультрамелкозернистая (УМЗ) структура. Анализ механизмов упрочнения, основанный на полученных новых сведениях о микроструктуре, показал, что основными причинами повышения прочности и пластичности УМЗ-сплава Zn–1%Li–2%Mg являются воздействия дисперсионного, зернограничного и гетеродеформационного типов упрочнения, включая дислокационный тип.

Ключевые слова: цинковый сплав, интенсивная пластическая деформация, прочность, пластичность, микроструктура, фазовый состав, рентгеноструктурный анализ, механизмы упрочнения.

Благодарности: Исследование выполнено за счет гранта Российского научного фонда № 23-29-00667,
https://rscf.ru/project/23-29-00667

Для цитирования: Ситдиков В.Д., Хафизова Э.Д., Поленок М.В. Влияние интенсивной пластической деформации на структуру и свойства сплава Zn–1%Li–2%Mg. *Известия вузов. Цветная металлургия*. 2023;29(6):35–43.
https://doi.org/10.17073/0021-3438-2023-6-35-43

Introduction

In recent years, there has been a growing focus among specialists on research aimed at developing and optimizing the physical and mechanical properties of new biodegradable zinc-based alloys for medical applications [1—5]. These materials possess the unique characteristic of complete dissolution within the body, obviating the need for repeated surgical interventions to remove implanted devices [6; 7].

Zinc, as a base material, is well-known for its relatively low ultimate tensile strength (σ_{ut} ~ 34 MPa) and low ductility (δ ~ 1.2 %) [8]. Consequently, substantial strengthening measures are required to ensure that the material meets the stringent clinical trial criteria for biodegradable stents. These criteria demand an ultimate tensile strength exceeding 300 MPa and a minimum ductility of 15 % [6]. To achieve these specifications, a range of techniques is employed, including alloying methods involving various impurity elements (such as Li, Mg, Mn, Ca, Cu), heat treatments, and different plastic deformation schemes [9—11].

Specifically, a study referenced in [10] established that the ultimate strength of zinc can be substantially enhanced, reaching 213 MPa, by alloying it with 0.8 wt.% of Li. The authors further demonstrated that a combination of alloying and extrusion processes can elevate the ultimate strength of the same alloy (Zn—0.8 wt.%[1] Li) to ~ 500 MPa, placing it on par with the strength level of stainless steel. Moreover, the study discovered that additional alloying of the Zn—Li alloy with Mg, followed by 4 cycles of hot extrusion, can push the ultimate tensile strength to a remarkable 647 MPa [10], marking an all-time high for zinc alloys.

Conversely, another study [12] demonstrated that by increasing the degree of zinc alloying with lithium to 6 at.% and employing a different deformation scheme (warm rolling), samples with enhanced ultimate strength (560 MPa) can be obtained. However, it's essential to note that in all of these studies [10; 12], the zinc alloys exhibited extremely low ductility, not exceeding 5 %. This limitation significantly restricts the range of potential applications for these materials.

In pursuit of enhancing the properties of zinc alloys, researchers are actively exploring novel approaches and thermomechanical processing techniques. These methods include severe plastic deformation (SPD) processes, such as Equal Channel Angular Pressing (ECAP) and High-Pressure Torsion (HPT), as mentioned in [13; 14]. The primary objective of these deformation schemes is to enhance the ductility of zinc alloys, while simultaneously refining the grain structure to the nanometer level, thereby creating high-strength materials. For example, as indicated in [15], the application of HPT treatment, even to pure zinc, results in a notable increase in ultimate strength, reaching 140 MPa, and an impressive ductility of 40 %. In a related study [14], it was observed that subjecting a doped zinc alloy, Zn—0.6Mg—0.1Ca, to ECAP (12 cycles) elevated its ultimate tensile strength to 300 MPa, along with an improved ductility of 20 %.

The paper referenced in [13] details the development of a high-strength alloy, boasting an ultimate tensile strength of 318 MPa and a remarkable ductility of 34 %, following four ECAP cycles of the Zn—1Cu—0.5Mg alloy. Furthermore, the authors demonstrated that by increasing the Cu doping level in the alloy to 3 % while applying the same processing methods, the ultimate tensile strength (σ_{ut}) rise to 358 MPa, was elevated to 358 MPa, and the ductility (δ) increased to an impressive 51 %.

The concise review highlights the capability to significantly enhance the ductility of zinc alloys by adjusting the degree of impurity element doping and optimizing the conditions and methods of SPD. Consequently, this paper aims to identify the specific conditions, including pressure, temperature, and degree of deformation, required for the high-pressure torsion method to create a unique ultra-fine-grained (UFG) structure in the Zn—1Li—2Mg alloy. This UFG structure is integral to achieving not only high strength but also exceptionally high ductility in the material.

Materials and methods

The research involved the casting of high-purity Zn—1Li—2Mg bioresorbable zinc alloy ingots. These ingots were then subjected to HPT to achieve optimal mechanical properties. The HPT was carried out at a pressure of 6 GPa, with the upper striker rotating at a speed of 1 revolution per minute. This resulted in the formation of disk-shaped samples, each 1.1 mm thick and with a radius of 10 mm. Furthermore, the level of deformation was adjusted by varying the number of HPT revolutions, ranging from 0.5 to 10, and the temperature, which was set between 27 °C and 150 °C. The accumulated deformation degree was calculated using the formula [16]:

$$\gamma = 2\pi Nr/h,$$

where h and r represent the thickness and the radius of the sample, respectively, mm, N is the number of revolutions applied in the HPT process.

To determine the mechanical properties of the alloy, small flat samples with a gauge length of 4 mm, a thickness of 1.0 mm, and a width of 1.0 mm were tested for elongation. These tests were conducted using a specialized testing machine, the Instron 8801 (UK). To assess the ductility of the alloy, the total extension of the sample was calculated using the following formula:

$$\delta = \Delta l \cdot 100\ \%/l,$$

where l is the length of the sample's gauge part, mm, Δl is the in the length of the sample's gauge part after the sample's destruction, mm.

During the alloy elongation tests, the incremental step was set at 10^{-4} mm, and the deformation rate was maintained at $4 \cdot 10^{-4}$ mm/s. Mechanical tests were conducted at least three times for each structural state of the alloy to ensure consistent and reliable results.

The microstructure of the alloy was analyzed using a Q250 scanning electron microscope (SEM) (Thermo Fisher Scientific, USA). The SEM operated with

[1] Hereinafter the content of alloy components is given in wt.%.

an accelerating voltage of electrons reaching 25 kV. The electron beam diameter was adjustable within the range of 1 to 5 μm, and the focal length was varied within the 8—10 mm range. During the analysis, the pressure in the chamber did not exceed 10^{-3} Pa.

To estimate the parameters of the alloy's fine structure, the *X*-ray diffraction (XRD) patterns were recorded and analyzed using a D8 Advance diffractometer (Bruker, Germany) in Bragg-Brentano geometry. The *X*-ray diffraction patterns were captured in the continuous mode at a rate of 1°/min, covering angles 2θ = 15°÷155°. The *X*-ray radiation source used was CuK_α, generated from a wide-focus *X*-ray tube with settings of $U = 40$ kV and $I = 40$ mA.

Qualitative *X*-ray phase analysis (XPA) was carried out using the EVAplus program (www.bruker.com) with reference to the PDF-2 diffractometric database. Additionally, quantitative analysis was performed to determine the phase ratios with the identified phases using the Rietveld method in TOPAS v.4.2 (www.bruker.com) [17].

Results and discussion

The results of mechanical tensile tests demonstrated that the parent Zn—1Li—2Mg alloy had the following properties: a yield strength σ_y ~ 150 MPa, an ultimate tensile strength σ_{ut} ~ 155 MPa, and a ductility $\delta \le 0.5$ % (See Table). HPT treatment at the room temperature with 10 revolutions ($\gamma = 571$) significantly improved the alloy's mechanical properties, increasing σ_y to 330 MPa and σ_{ut} to 409 MPa, while also enhancing ductility to 47 %.

By further varying the temperature and HPT degree, a specific regime (150 °C, 10 revolutions, $\gamma = 571$), at which the alloy exhibited remarkable mechanical properties (σ_y ~ 385 MPa, σ_{ut} ~ 490 MPa, and $\delta = 44$ %), was identified. Notably, during the initial HPT stages (up to 0.5—1.0 revolutions, $\gamma = 28.5 \div 57.1$), the samples also exhibited increased strength, reaching up to 500 MPa, but their ductility did not surpass 7 %.

Mechanical properties of the Zn–Li–2Mg alloy in the initial state and after HPT treatment

Механические свойства сплава Zn–1Li–2Mg в исходном состоянии и после обработки

State	σ_y, MPa	σ_{ut}, MPa	δ, %
Initial	149	155	0.4
HPT 10 rev., $\gamma = 571$, $t = 27$ °C	330	409	47
HPT 10 rev., $\gamma = 571$, $t = 150$ °C	385	490	44

To investigate the simultaneous increase in strength and ductility of the studied alloy, a microstructure analysis using SEM and XPA methods was conducted.

In the initial (cast) state, the alloy's microstructure exhibits both light and dark regions (Fig. 1, *a*, *b*). Based on the Zn—Li phase diagram [18] and the characteristics of SEM and XPA methods, we identify the light regions (oval shape and layered structure) as a mixture of Zn and β-$LiZn_4$ eutectic phases, while the dark regions correspond to the primary β-$LiZn_4$ phase. At the interface between these phases, bright regions (inset in Fig. 1, *b*) are occasionally observed, which, according to elemental mapping data, indicate the presence of the $MgZn_2$ phase. Furthermore, a detailed analysis of impurity atom distribution was conducted through linear mapping along the yellow line (Fig. 1, *c*). The results, showing the mass distribution of Mg and Zn atoms along the selected line, are depicted in Fig. 1, *d*. The graph reveals a slight increase in Mg atom content in the dark regions. According to the Zn—Mg phase diagram at 2 wt.% Mg in Zn at room temperature, the mixture should contain the Zn and Mg_2Zn_{11} phases [19]. However, our XPA data, as presented below, did not detect the Mg_2Zn_{11} phase in the initial alloy state. This suggests that, in addition to the $MgZn_2$ phase, Mg atoms may exist as impurities within the primary β-$LiZn_4$.

After HPT treatment at both room temperature and 150 °C (Fig. 2, *a*, *b*), significant changes occur in the microstructure of the analyzed alloy, leading to the emergence of a banded structure. According to XPA data and existing literature [13, 20], this structure is formed by Zn phases, as well as mixtures of α-Zn + ~$LiZn_3$ and α-Zn + Mg_2Zn_{11}. Magnified images of the detected phases in the post-HPT states are presented in Fig. 2, *c*, *d*. Following HPT at 150 °C, spherically shaped Mg_2Zn_{11} phase particles (dark regions) are observed falling out in bright bands that correspond to the Mg_2Zn_{11} phase (upper right inset in Fig. 2, *d*), in agreement with prior research [7; 13]. After HPT treatment at room temperature, the structure retains remnants of lamellar eutectics, consisting of alternating light Zn lamellae and dark Mg_2Zn_{11} lamellae (inset in Fig. 2, *c*) with an average thickness of 360 nm and 140 nm, respectively (Fig. 2, *c*). Meanwhile, the diameter of spherical Mg_2Zn_{11} particles in the Zn phase was ~300 nm.

According to the sources [21; 22], warm rolling of the Zn—Li alloy results in the formation of string-like β-$LiZn_4$ particles, creating a fine-scale network in the Zn phase, with needle-like Zn particles precipitating in the β-$LiZn_4$ phase. Our research revealed that HPT

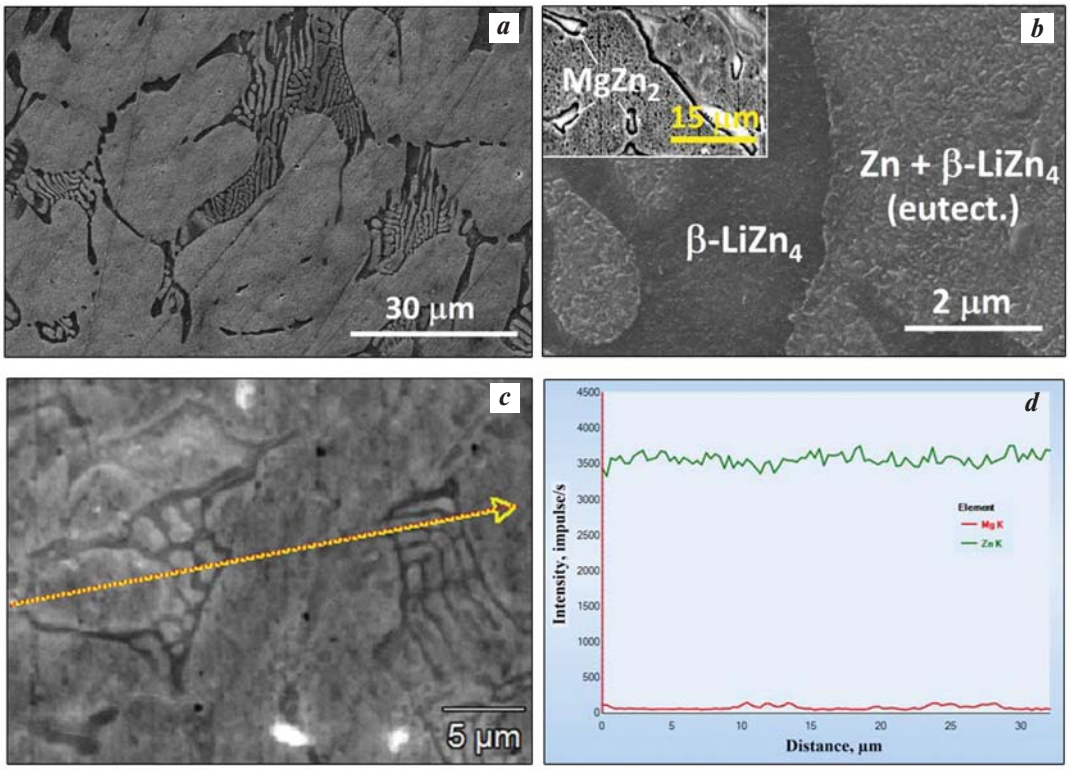

Fig. 1. SEM images of the Zn–1Li–2Mg initial alloy microstructure
a – magnification 4000×, ***b*** – 50000×, ***c*** – linear mapping region, ***d*** – distribution of Mg and Zn atoms along the line highlighted in Fig. ***c***

Рис. 1. РЭМ-изображения микроструктуры Zn–1Li–2Mg исходного сплава
a – увеличение 4000×, ***b*** – 50000×, ***c*** – участок проведения линейного картирования,
d – распределение атомов Mg и Zn вдоль выделенной на рис. ***c*** линии

treatment of the alloy leads to the precipitation of spherically shaped β-$LiZn_4$ particles in the Zn phase (inset in Fig. 2, *a*, *b*).

In the β-$LiZn_4$ phase, apart from the large cylindrical Zn particles, small spherical Zn particles (lower inset in Fig. 2, *c*) with a diameter of ~ 80 nm also precipitate. Similar-shaped precipitations were previously observed in the lightly doped Zn—0.8Li—0.1Mg alloy subjected to HPT [23]. Detailed analysis reveals that HPT treatment at room temperature is more effective in refining the grain structure of the Zn phase compared to HPT at 150 °C (see Fig. 2, *a*, *b* and insets). In the former case, the Zn phase consists of equiaxial nanoscale grains, with an average size of 360 nm after HPT at 27 °C, while it reaches 610 nm after HPT at 150 °C.

Figure 3 displays the *X*-ray diffraction patterns of the alloy in its initial (cast) state and after 10 revolutions of HPT (γ = 571) at different temperatures. Qualitative XPA analysis reveals responses related to Zn, ~$LiZn_3$, β-$LiZn_4$, Mg_2Zn_{11}, and $MgZn_2$ phases. in the *X*-ray diffraction patterns of the zinc alloy. Quantitative XPA analysis indicates that in the initial state, the Zn phase constitutes 31.3 % of the alloy, while the fractions of ~$LiZn_3$, β-$LiZn_4$, and $MgZn_2$ phases are 45, 11.8, and 11.9 %, respectively. After 10 revolutions of HPT (γ = = 571) at t = 27 °C, the Zn content significantly increases to 52.4 %, while the ~$LiZn_3$ phase decreases to 21.7 %. Furthermore, the fractions of β-$LiZn_4$ and $MgZn_2$ phases decrease to 7.2 % and 0.5 %, respectively. Notably, in contrast to the initial alloy, HPT treatment at this temperature results in the formation of the Mg_2Zn_{11} phase, with a relatively high concentration of 18.2 % in the alloy.

When the deformation temperature is increased to 150 °C and 10 revolutions of HPT processing are applied (γ = 571), the mass fractions of Zn and Mg_2Zn_{11} phases further increase to 57.7 % and 21.5 %, respectively. Simultaneously, the contents of other phases continue to decrease: ~$LiZn_3$ (16.3 %), β-$LiZn_4$ (4.2 %), and $MgZn_2$ (0.3 %). Quantitative phase ratios were determined by analyzing the *X*-ray diffraction patterns using the Rietveld method. An example of the processed region of the alloy's *X*-ray diffraction pattern after 10 revolutions of HPT (γ = 571, t = 150 °C) is shown in Fig. 3, *b*.

The unique mechanical properties observed in samples subjected to HPT can be attributed to hardening

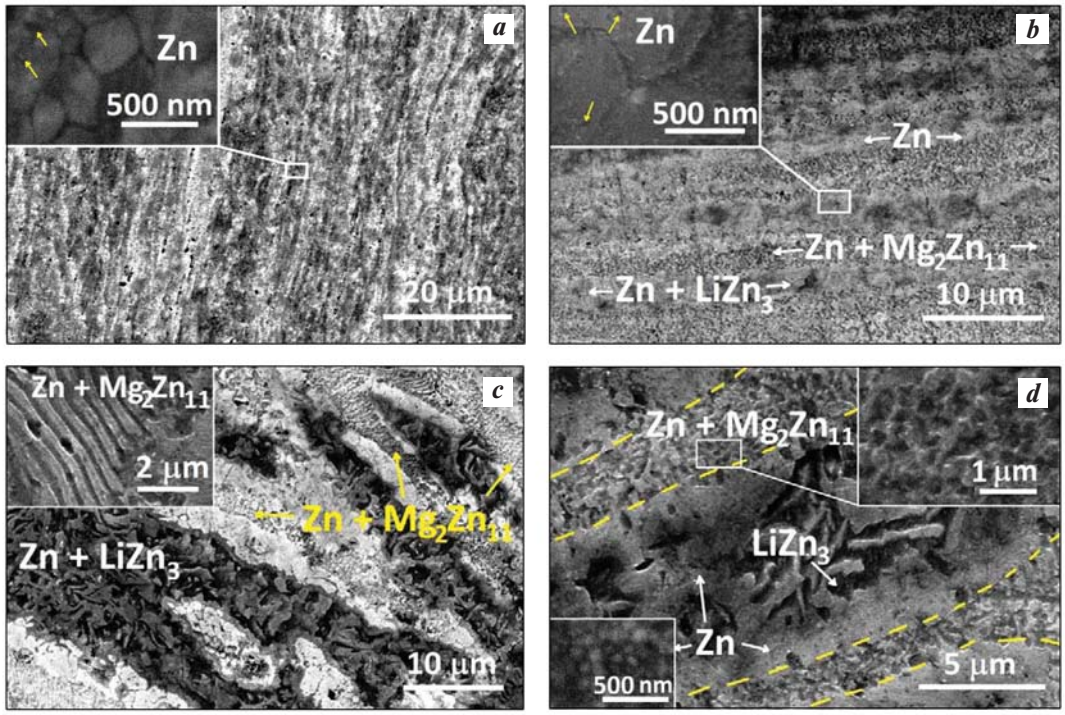

Fig. 2. SEM images of the Zn–1Li–2Mg alloy microstructure after HPT treatment:

a – HPT (t = 27 °C, 10 rev., γ = 571), magnification 5000×, the insert shows the Zn phase;
b – HPT (150 °C, 10 rev., γ = 571), magnification 10000×, the insert shows the Zn phase;
c – HPT (t = 27 °C, 10 rev., γ = 571), magnification 8000×, the insert shows Zn and Mg_2Zn_{11} phases;
d – HPT (150°C, 10 rev., γ = 571), magnification 20000×, inserts show Zn and Mg_2Zn_{11} particles

Рис. 2. РЭМ-изображения микроструктуры сплава Zn–1Li–2Mg после обработки

a – ИПДК (t = 27 °C, 10 об., γ = 571), увеличение 5000×, на вставке – фаза Zn;
b – ИПДК (150 °C, 10 об., γ = 571), 10000×, на вставке – фаза Zn;
c – ИПДК (t = 27 °C, 10 об., γ = 571), 8000×, на вставке – пластины фаз Zn и Mg_2Zn_{11};
d – ИПДК (150 °C, 10 об., γ = 571), 20000×, на вставках – частицы Zn и Mg_2Zn_{11}

mechanisms, as supported by the microstructure analysis described earlier. SEM and XRD studies revealed the precipitation of Zn, β-$LiZn_4$, and Mg_2Zn_{11} particles during HPT treatment of the Zn-alloy. It was noted that at higher deformation temperatures, such as 150 °C, the quantity and size of these precipitates increase compared to room temperature HPT. This suggests increased diffusion processes' activity at elevated HPT temperatures, leading to more comprehensive dynamic. In general, it can be concluded that the dispersion mechanism significantly contributes to alloy hardening during HPT, and this effect intensifies with a higher precipitate content [3; 5].

Additionally, another hardening mechanism at play in the zinc alloy is grain boundary strengthening resulting from grain structure refinement. Grains ground to nanometer sizes not only enhance strength but can also increase the alloy's ductility by activating grain boundary sliding processes [25; 26]. This mechanism, well-documented in literature [25], is known to be the predominant superductility mechanism in UFG zinc alloys and is typically activated at grain sizes less than 1 μm.

In a study by [26], refining the grain structure of the Zn—22Al alloy to 700—900 nm using the ECAP method led to a remarkable increase in ductility, reaching 280 %. Our research has similarly shown that the primary phase in HPT treatment is zinc with nanometer-sized grains (Fig. 2, *a*, *b*), with an increased fraction of grain boundaries contributing to enhanced ductility. This suggests that the grain refinement in the zinc phase not only strengthens the alloy but also explains its improved ductility.

Another notable strengthening mechanism in UFG metallic materials is hetero-deformation induced hardening [27]. This mechanism is observed in metals and alloys where heterostructured materials form, comprising separate domains that vary significantly in strength. Extreme plastic deformations generate back stress within the material structure due to the superposition of forward and reverse stresses from hard and soft domains in

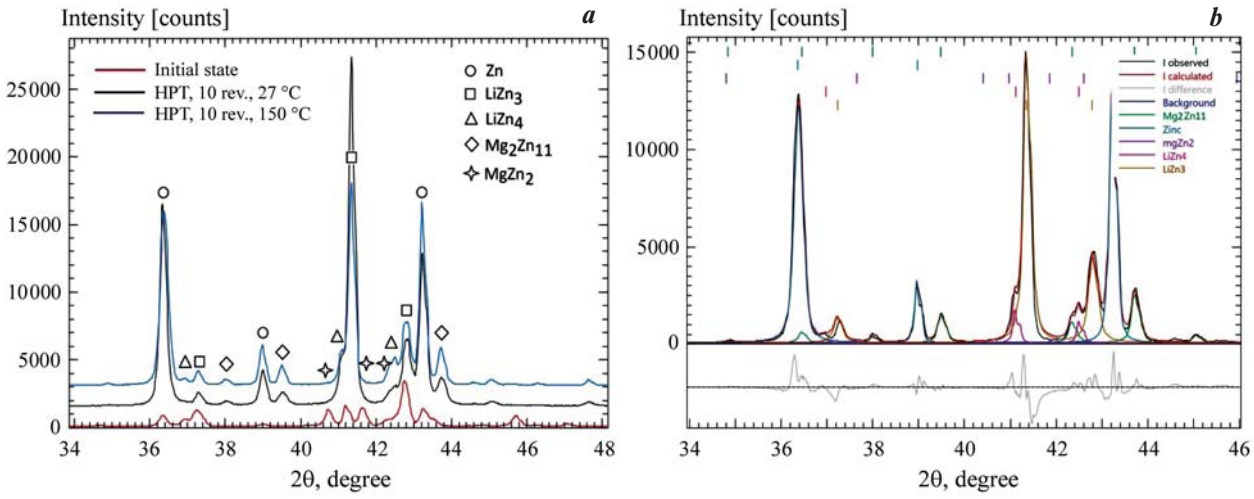

Fig. 3. *X*-ray diffraction patterns of the initial and HPT-processed alloys (***a***), as well as the analyzed section of the *X*-ray diffraction pattern after HPT treatment (10 rev., γ = 571, *t* = 150 °C) (***b***)

Рис. 3. Дифрактограммы исходного и ИПДК-обработанного сплавов (***a***), а также проанализированный участок дифрактограммы образца после ИПДК (10 об., γ = 571, *t* = 150 °C) (***b***)

the microstructure [27]. Long-range back stresses, created by clusters and pile-ups of dislocations, strengthen the soft domains, contributing to an overall increase in strength [27].

In cases where HPT is performed at high RPM, a band structure forms, including α-Zn phases, a mixture of α-Zn phases and the ~$LiZn_3$ phase, as well as the α-Zn phase with Mg_2Zn_{11} particles precipitating. These phases exhibit different microhardness levels and can be considered as soft and hard domains or phases. Our studies [23] have shown that the soft phase of Zn in the Zn—Li—Mg alloy is characterized by an increased dislocation density. Consequently, the mechanism of hetero-deformation induced hardening, which includes dislocation strengthening, is also an active force at high RPMs during HPT.

Conclusion

After optimizing the HPT parameters, a unique regime (pressure 6 GPa, temperature 150 °C, 10 revolutions, γ = 571) was discovered, resulting in the Zn—1Li—2Mg alloy exhibiting exceptional mechanical properties. These properties include a yield strength of ~385 MPa, an ultimate tensile strength of ~ 490 MPa, and ductility reaching 44 %.

Detailed analysis of the alloy's microstructure revealed the formation of a distinctive band structure. This structure comprises the α-Zn phase, a mixture of α-Zn phase and ~$LiZn_3$ phases, as well as the α-Zn phase with Mg_2Zn_{11} particles. Notably, Zn particles were found to precipitate in the ~$LiZn_3$ phase, while Mg_2Zn_{11} and β-$LiZn_4$ particles precipitated in the Zn phase. Additionally, the application of HPT treatment resulted in the formation of an UFG structure in the primary Zn phase.

The analysis of hardening mechanisms identified the key factors contributing to the enhanced strength of the Zn—1Li—2Mg alloy with a UFG structure. These mechanisms include dispersion, grain boundary strengthening, and hetero-deformation induced hardening, which involves dislocation strengthening. Moreover, the alloy's improved ductility can be attributed to the extremely small grain size of the Zn phase, which promotes the activation of grain boundary sliding processes.

References

1. Hernández-Escobar D., Champagne S., Yilmazer H., Dikici B., Boehlert C.J., Hermawan H. Current status and perspectives of zinc-based absorbable alloys for biomedical applications. *Acta Materialia*. 2019;(97):1—22. https://doi.org/10.1016/j.actbio.2019.07.034
2. Huang S., Wang L., ZhengY., Qiao L., Yan Y. In vitro degradation behavior of novel Zn—Cu—Li alloys: Roles of alloy composition and rolling processing. *Materials & Design*. 2021;(212):110288. https://doi.org/10.1016/j.matdes.2021.110288
3. Li W., Dai Y., Zhang D., Lin J., Biodegradable Zn—0.5Li alloys with supersaturated solid solution-aging treatment for implant applications. *Journal of Materials Research and Technology*. 2023;(24):9292—9305. https://doi.org/10.1016/j.jmrt.2023.05.136

4. Yang L., Li X., Yang L., Zhu X., Wang M., Song Z., Liu H.H., Sun W., Dong R., Yue J. Effect of Mg contents on the microstructure, mechanical properties and cytocompatibility of degradable Zn—0.5Mn—*x*Mg alloy. *Journal of Functional Biomaterials*. 2023;(14):195. https://doi.org/10.3390/jfb14040195
5. Ye L., Huang H., Sun C., Zhuo X., Dong Q., Liu H., Ju J., Xue F., Bai J., Jiang J. Effect of grain size and volume fraction of eutectic structure on mechanical properties and corrosion behavior of as-cast Zn—Mg binary alloys. *Journal of Materials Research and Technology*. 2022;(16):1673—1685. https://doi.org/10.1016/j.jmrt.2021.12.101
6. Yuan W., Xia D., Wu S., Zheng Y., Guan, Z., Rau J.V. A review on current research status of the surface modification of Zn-based biodegradable metals. *Bioactive Materials*. 2022;(7):192—216. https://doi.org/10.1016/j.bioactmat.2021.05.018
7. García-Mintegui C., Córdoba L.C., Buxadera-Palomero J., Marquina A., Jiménez-Piqué E., Ginebra M.P., Cortina J.L., Pegueroles M. Zn—Mg and Zn—Cu alloys for stenting applications: From nanoscale mechanical characterization to in vitro degradation and biocompatibility. *Bioactive Materials*. 2021;6(12):4430—4446. https://doi.org/10.1016/j.bioactmat.2021.04.015
8. Tong X., Zhang D., Zhang X., Su Y., Shi Z., Wang K., Lin J., Li Y., Lin J., Wen C. Microstructure, mechanical properties, biocompatibility, and in vitro corrosion and degradation behavior of a new Zn—5Ge alloy for biodegradable implant materials. *Acta Biomaterialia*. 2018;(82):197—204. https://doi.org/10.1016/j.actbio.2018.10.015
9. Yang H., Jia B., Zhang Z., Qu X., Li G., Lin W., Zhu D., Dai K., Zheng Y. Alloying design of biodegradable zinc as promising bone implants for load-bearing applications. *Nature Communications*. 2020;(11):401. https://doi.org/10.1038/s41467-019-14153-7
10. Li Zh., Shi Zh.-Zh., Hao Y., Li H., Zhang H., Liu X., Wang L.-N. Insight into role and mechanism of Li on the key aspects of biodegradable Zn—Li alloys: Microstructure evolution, mechanical properties, corrosion behavior and cytotoxicity. *Materials Science and Engineering: C*. 2020;(114):111049. https://doi.org/10.1016/j.msec.2020.111049
11. Ye L., Liu H., Sun C., Zhuo X., Ju J.; Xue F., Bai J., Jiang J., Xin Y. Achieving high strength, excellent ductility, and suitable biodegradability in a Zn—0.1Mg alloy using room-temperature ECAP. *Journal of Alloys and Compounds*. 2022;(926):166906. https://doi.org/10.1016/j.jallcom.2022.166906
12. Zhao S., McNamara C.T., Bowen P.K., Verhun N., Braykovich J.P., Goldman J., Drelich J.W. Structural characteristics and in vitro biodegradation of a novel Zn—Li alloy prepared by induction melting and hot rolling. *Metallurgical and Materials Transactions A*. 2017;(48):1204—1215. https://doi.org/10.1007/s11661-016-3901-0
13. Liu H., Ye L., Ren K., Sun C., Zhuo X., Yan K., Ju J., Jiang J., Xue F., Bai J. Evolutions of $CuZn_5$ and Mg_2Zn_{11} phases during ECAP and their impact on mechanical properties of Zn—Cu—Mg alloys. *Journal of Materials Research and Technology*. 2022;(21):5032—5044. https://doi.org/10.1016/j.jmrt.2022.11.095
14. Huang H., Liu H., Wang L., Yan K., Li Y., Jiang J., Ma A., Xue F., Bai J. Revealing the effect of minor Ca and Sr additions on microstructure evolution and mechanical properties of Zn—0.6 Mg alloy during multi-pass equal channel angular pressing. *Journal of Alloys and Compounds*. 2020;(844):155923. https://doi.org/10.1016/j.jallcom.2020.155923
15. Polenok M.V., Khafizova E.D., Islamgaliev R.K. Influence of severe plastic deformation on the mechanical properties of pure zinc. *Frontier Materials & Technologies*. 2022;(3—2):25—31. https://doi.org/10.18323/2782-4039-2022-3-2-25-31
16. Valiev R.Z., Islamgaliev R.K., Alexandrov I.V. Bulk nanostructured materials from severe plastic deformation. *Progress Materials Science*. 2000;45(2):103—189. https://doi.org/10.1016/S0079-6425(99)00007-9
17. Rietveld H.M. A profile refinement method for nuclear and magnetic structures. *Journal of Applied Crystallography*. 1969;2(2):65—71. https://doi.org/10.1107/S0021889869006558
18. Pelton A. The Li—Zn (Lithium—Zinc) system. *Journal of Phase Equilibria*. 1991;(12):42—45. https://doi.org/10.1007/BF02663672
19. Liu S., Kent D., Doan N., Dargusch M., Wang G. Effects of deformation twinning on the mechanical properties of biodegradable Zn—Mg alloys. *Bioactive Materials*. 2018;4(1):8—16. https://doi.org/10.1016/j.bioactmat.2018.11.001
20. Zhang Y., Yan Y., Xu X., Lu Y., Chen L., Li D., Dai Y., Kang Y., Yu K., Investigation on the microstructure, mechanical properties, in vitro degradation behavior and biocompatibility of newly developed Zn—0.8%Li—(Mg, Ag) alloys for guided bone regeneration. *Materials Science and Engineering: C*. 2019;(99):1021—1034. https://doi.org/10.1016/j.msec.2019.01.120
21. Shi Z.Z., Gao X.X., Zhang H.J., Liu X.F., Li H.Y., Zhou C., Yin Y.X., Wang L.N. Design biodegradable Zn alloys: Second phases and their significant influences on alloy properties. *Bioactive Materials*. 2020;5(2):210—218. https://doi.org/10.1016/j.bioactmat.2020.02.010
22. Li Zh., Shi Zh.-Zh., Zhang H.-J., Li H.-F., Feng Y., Wang L.-N. Hierarchical microstructure and two-stage corro-

sion behavior of a high-performance near-eutectic Zn—Li alloy. *Journal of Materials Research and Technology*. 2021; 80:50—65. https://doi.org/10.1016/j.jmst.2020.10.076
23. Sitdikov V.D., Kulyasova O.B., Sitdikova G.F., Islamgaliev R.K., Yufeng J. Structural-phase transformations in a Zn—Li—Mg alloy subjected to severe plastic deformation by torsion. *Frontier Materials & Technologies*. 2022;(3—2): 44—55. https://doi.org/10.18323/2782-4039-2022-3-2-44-55
24. Zhuo X., Wu Y., Ju J., Liu H., Jiang J., Hu Z., Bai J., Xue F. Recent progress of novel biodegradable zinc alloys: from the perspective of strengthening and toughening. *Journal of Materials Research and Technology*. 2022;(17):244—269. https://doi.org/10.1016/j.jmrt.2022
25. Demirtas M., Yanar H., Saray O., Pürçek G. Room temperature superplasticity in fine/ultrafine-grained Zn—Al alloys with different phase compositions. *Defect and Diffusion Forum*. 2018;(85):72—77. https://doi.org/10.4028/www.scientific.net/ddf.385.72
26. Kumar P., Xu C., Langdon T.G. Mechanical characteristics of a Zn—22%Al alloy processed to very high strains by ECAP. *Materials Science and Engineering A*. 2006; (429): 324—328. https://doi.org/10.1016/j.msea.2006.05.044
27. Zhu Y.T., Wu X.L. Perspective on hetero-deformation induced (HDI) hardening and back stress. *Materials Research Letters*. 2019;(7): 393—398. https://doi.org/10.1080/21663831.2019.1616331

Information about the authors

Vil' D. Sitdikov – Dr. Sci. (Phys.-Math.), Expert of RN-BashNIPIneft LLC; Senior Researcher at the Institute of Physics of Molecules and Crystals of the Ufa Scientific Center of the Russian Academy of Sciences (IPMC USC RAS).
https://orcid.org/0000-0002-9948-1099
E-mail: svil@ugatu.su, SitdikovVD@bnipi.rosneft.ru

El'vira D. Khafizova – Cand. Sci. (Eng.), Senior Researcher of IPMC USC RAS; Associate Professor of the Department of Materials Science and Physics of Metals, Senior Researcher at the Research Laboratory "Metals and Alloys under Extreme Impacts", Ufa University of Science and Technologies.
https://orcid.org/0000-0002-4618-412X
E-mail: ela.90@mail.ru

Milena V. Polenok – Laboratory Assistant of IPMC USC RAS; Undergraduate, Research Engineer at the Research Laboratory "Metals and Alloys under Extreme Impacts", Ufa University of Science and Technologies.
https://orcid.org/0000-0001-9774-1689
E-mail: renaweiwei.179@mail.ru

Информация об авторах

Виль Даянович Ситдиков – д.ф.-м.н., эксперт ООО «РН-БашНИПИнефть»; ст. науч. сотрудник Института физики молекул и кристаллов Уфимского научного центра Российской академии наук (ИФМК УНЦ РАН).
https://orcid.org/0000-0002-9948-1099
E-mail: svil@ugatu.su, SitdikovVD@bnipi.rosneft.ru

Эльвира Динифовна Хафизова – к.т.н., ст. науч. сотрудник ИФМК УНЦ РАН; доцент кафедры материаловедения и физики металлов, ст. науч. сотрудник НИЛ «Металлы и сплавы при экстремальных воздействиях» Уфимского университета науки и технологий (УУНиТ).
https://orcid.org/0000-0002-4618-412X
E-mail: ela.90@mail.ru

Милена Владиславовна Поленок – лаборант ИФМК УНЦ РАН; инженер-исследователь НИЛ «Металлы и сплавы при экстремальных воздействиях» УУНиТ.
https://orcid.org/0000-0001-9774-1689
E-mail: renaweiwei.179@mail.ru

Contribution of the authors

V.D. Sitdikov – determined the purpose of the work, analyzed the experiments, wrote the article.

E.D. Khafizova – conducted *X*-ray phase analysis, conducted SEM analysis, participated in the discussion of the results.

M.V. Polenok – preparation of samples, carried out HPT processing, carried out mechanical tests, participated in the discussion of the results.

Вклад авторов

В.Д. Ситдиков – определение цели работы, анализ экспериментов, написание текста статьи.

Э.Д. Хафизова – проведение рентгенофазового и РЭМ анализов, участие в обсуждении результатов.

М.В. Поленок – подготовка образцов, проведение ИПДК-обработки и механических испытаний, участие в обсуждении результатов.

The article was submitted 10.07.2023, revised 20.09.2023, accepted for publication 25.09.2023

Статья поступила в редакцию 10.07.2023, доработана 20.09.2023, подписана в печать 25.09.2023